THE JOURNAL OF BIOLOGICAL CHEMISTRY
Vol. 274, No. 15, Issue of April 9, pp. 10213–10218, 1999

Printed in U.S.A.

Chloroquine Binds in the Cofactor Binding Site of *Plasmodium falciparum* Lactate Dehydrogenase*

(Received for publication, August 25, 1998, and in revised form, December 8, 1998)

Jon A. Read, Kay W. Wilkinson, Rebecca Tranter‡, Richard B. Sessions, and R. Leo Brady§

From the Department of Biochemistry and Centre for Molecular Recognition, University of Bristol, Bristol BS8 1TD United Kingdom

Although the molecular mechanism by which chloroquine exerts its effects on the malarial parasite *Plasmodium falciparum* remains unclear, the drug has previously been found to interact specifically with the glycolytic enzyme lactate dehydrogenase from the parasite. In this study we have determined the crystal structure of the complex between chloroquine and *P. falciparum* lactate dehydrogenase. The bound chloroquine is clearly seen within the NADH binding pocket of the enzyme, occupying a position similar to that of the adenyl ring of the cofactor. Chloroquine hence competes with NADH for binding to the enzyme, acting as a competitive inhibitor for this critical glycolytic enzyme. Specific interactions between the drug and amino acids unique to the malarial form of the enzyme suggest this binding is selective. Inhibition studies confirm that chloroquine acts as a weak inhibitor of lactate dehydrogenase, with mild selectivity for the parasite enzyme. As chloroquine has been shown to accumulate to millimolar concentrations within the food vacuole in the gut of the parasite, even low levels of inhibition may contribute to the biological efficacy of the drug. The structure of this enzyme-inhibitor complex provides a template from which the quinoline moiety might be modified to develop more efficient inhibitors of the enzyme.

Malaria is one of the major diseases of mankind, claiming 3 million lives worldwide annually. Resistance to existing antimalarial drugs is a large and increasing problem. Recently we have determined the first high-resolution structure of an enzyme from the *Plasmodium falciparum* parasite, the causative agent of malaria. This 1.7-Å structure (1) of the essential glycolytic enzyme *P. falciparum* lactate dehydrogenase (pfLDH)[1] has revealed a unique cleft adjacent to the active site, ideally suited as a target for the rational design of inhibitors. Another feature of the structure is a significant displacement of the NADH cofactor relative to other forms of LDH, reflecting that the malarial enzyme has a unique mode of association with the cofactor and hence a distinctive NADH binding pocket. These features suggest pfLDH may form an appropriate target for structure-based design of novel antimalarials.

Chloroquine (CQ, Fig. 1, *left*) and related quinoline compounds have been used extensively throughout the world as prophylactics to prevent the development of malaria. Although the mechanism of action of CQ on the parasite is not completely understood, it is thought to interfere with the function of the food vacuole in the mature stages of the erythrocytic parasite (2). CQ is a weak base and accumulates to high concentrations within the acidic food vacuole (3). Within these vacuoles, hemoglobin is degraded by proteases to provide a supply of amino acids for the parasite, but also producing toxic heme moieties as a by-product (hematin; Fig. 1, *right*). The parasite normally detoxifies hematin by polymerizing the by-product to hemozoin, although the details of this process are unclear. Because CQ is known to bind to hematin, it was thought to exert its antimalarial activity by forming a complex with hematin, which inhibits its sequestration into hemozoin (4). Free heme causes cell lysis, and so CQ complexation with hematin was thought to be toxic to the parasite. This hypothesis is no longer favored because of the failure to show the existence of free heme in parasite cells. It has also been suggested that the target for CQ is a protein or proteins involved in the digestion or disposal of hemoglobin (5), although no target has been identified. CQ resistance is an increasingly serious problem and appears to correlate with decreased accumulation of the drug by CQ-resistant parasites. Identifying and understanding the interaction of proteins with CQ could lead the way to the development of new antimalarials to overcome these problems.

Intriguingly, recent studies (6) showed that photoreactive analogues of chloroquine interacted specifically with two proteins in infected red blood cells, one of which was identified (7) as pfLDH. In these studies some evidence for CQ binding to pfLDH was found, but it was not observed to inhibit the activity of pfLDH. However, CQ was found to modulate the inhibitory effect of hematin on LDH. Hematin itself strongly inhibits the malarial form of the enzyme (K_i = 0.2 μM), about 100-fold tighter than its binding to mammalian forms of the enzyme (K_i = 23 μM for bovine LDH). Equimolar amounts of CQ modestly decreased inhibition of the mammalian form by hematin by about 50% (K_i = 33 μM), whereas inhibition of the malarial enzyme was reduced by at least 2 orders of magnitude in the presence of CQ. This protective effect of CQ is most likely because of the formation of a tight complex between CQ and hematin (8), this complex binding less strongly to LDH than does free hemin itself.

In this study the crystal structure of the complex formed between chloroquine and pfLDH has been determined to assess the mode and the likely significance of this interaction. Additionally, the structure of this complex could provide a valuable starting point for structure-based modification of the quinoline skeleton for the development of novel antimalarials. This is of

* The costs of publication of this article were defrayed in part by the payment of page charges. This article must therefore be hereby marked "*advertisement*" in accordance with 18 U.S.C. Section 1734 solely to indicate this fact.

The atomic coordinates and structure factors (codes 1 ceq and 1 cet) have been deposited in the Protein Data Bank, Brookhaven National Laboratory, Upton, NY.

‡ Supported by a CASE Studentship from the Biotechnology and Biological Sciences Research Council (BBSRC) UK.

§ To whom correspondence should be addressed. Tel.: 44-117-928 7436; Fax: 44-117-928 8274; E-mail: L.Brady@bristol.ac.uk.

[1] The abbreviations used are: pfLDH, *P. falciparum* lactate dehydrogenase; LDH, lactate dehydrogenase; apo-pfLDH, apo form of pfLDH with no cofactor or substrate bound; CQ, chloroquine.

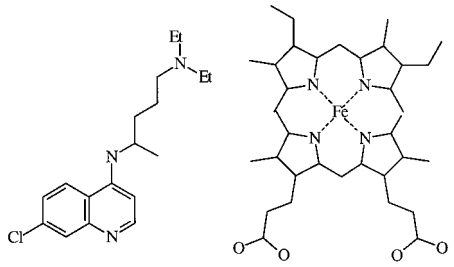

FIG. 1. **Molecular structures of (*left*) chloroquine and (*right*) hematin.**

particular interest as the quinoline family of compounds on which CQ is based are widely available, synthetically accessible, generally orally bioavailable, and of low toxicity. In combination with inhibition assays, these studies confirm the presence of a specific binding site for chloroquine in the malarial form of the enzyme, and provide guidance for modification of the quinoline structure to form an effective, selective, and competitive inhibitor for this crucial malarial enzyme.

EXPERIMENTAL PROCEDURES

Protein Production and Crystallization—Recombinant pfLDH and pig muscle LDH were expressed in *Escherichia coli* as described previously (1). Pig LDH is extremely similar to human LDH in sequence, structure, and activity and, because it is more readily available, was used as a representative form of mammalian LDH in this study. The fully activated forms of each enzyme were purified in a single step by affinity chromatography on an oxamate agarose column with NADH (9). Bound NADH was removed by dialysis against charcoal until the A_{280}/A_{260} measured above 1.9.

Crystals of the apo form of pfLDH (apo-pfLDH) were obtained at 18 °C by hanging drop vapor diffusion against a well containing 30% v/v 2-methyl-2,4-pentanediol, 200 mM sodium citrate, and 100 mM HEPES, pH 7.5. The protein concentration was 50 mg ml^{-1}. Crystals of the pfLDH·CQ complex were obtained by soaking crystals of apo-pfLDH for 72 h in mother liquor containing 5 mM chloroquine.

Structure Determination—Crystals of the CQ complex belong to the space group I222 with cell dimensions a = 79.9 Å, b = 85.4 Å, and c = 92.2 Å. The apo-LDH crystals have the same space group with cell dimensions of a = 79.8 Å, b = 85.6Å, and c = 91.8 Å. Crystals were mounted in Hampton research cryoloops and frozen using an Oxford Cryosystems Cryostream. Crystals were frozen in mother liquor only. Data were collected on a Nonius Dip-2000 Image Plate at 100 K using Cu-Kα radiation, filtered with mirrors, from a Nonius FR591 rotating anode generator operated at 45 kV and 95 mA. Data were processed using DENZO (10) and are summarized in Table I. The structures were solved by molecular replacement with AMORE (11) using the coordinates from the ternary pfLDH structure (1) from the Brookhaven Protein Data bank (code 1ldg) after removal of the cofactor and substrate analogue. The CQ·pfLDH complex structure was refined using iterative cycles of XPLOR (12) interspersed with manual rebuilding with QUANTA (MSI), and the apo-pfLDH structure using REFMAC (11) and O (13). Statistics for the final models are summarized in Table I.

Inhibition Studies—pfLDH activity was measured by monitoring the change in absorbance at 370 nm, associated with the reduction of NADH during the catalytic cycle. This wavelength was selected to avoid the strong absorbance of CQ at 340 nm. Absorbance changes over time (Fig. 2) were monitored using a Perkin-Elmer Lambda-2 spectrophotometer with assay conditions of 100 μM pyruvate and a range of NADH concentrations between 20 and 160 μM, in 50 mM phosphate buffer, pH 7.0, with a protein concentration of 10 nM. Inhibition was monitored by measuring rates in the presence of CQ at concentrations between 0.8 and 12.8 mM.

RESULTS

Both the apo and CQ complex forms of pfLDH adopt very similar overall structures (Fig. 3) with, in the absence of cofactor and substrate, characteristically open cofactor binding sites and disordered substrate specificity loops (residues 102–108). The root mean square deviation in all equivalent Cα positions between the two structures is 0.17 Å.

TABLE I

Summary of statistics for data collection and processing and for the refined models of both the apo form of pfLDH and the CQ · pfLDH complex

R_{merge} = $|\Sigma I_{obs} - I_{avg}|/\Sigma I_{avg}$; R-factor = standard crystallographic R-factor calculated on intensities; R-free = R-factor for a subset of reflections omitted from the refinement (20).

	Apo-pfLDH	CQ · pfLDH complex
Resolution range	20–2.0 Å	20–2.05 Å
R_{merge}	10.1%	6.7%
Redundancy	2.6	2.3
Completeness	89.9	99.8
$<I>/<\sigma I>$	7.0	16.3
Number of unique reflections	19,381	20,155
Number of reflections used in refinement	18,800	17,783
Number of reflections in free R set	581	1008
Number of atoms refined (protein)	2379	2293
Number of waters	187	250
R-factor	19.0%	15.4%
R-free	23.8%	19.3%
Average B_{iso} for protein atoms (Å^2)	14.0	11.3
Average B_{iso} for waters (Å^2)	21.1	22.0
Overall B_{iso} (Å^2)	14.6	12.4
r.m.s. deviation for bond length (Å)	0.007	0.006
r.m.s. deviation for bond angles (Å)	0.023	0.023

Prominent density for the quinoline ring was evident in the initial electron density maps from crystals of the complex (Fig. 4*a*), and assignment of the bound conformation of CQ was straightforward. There is no density for atoms beyond the second carbon atom of the 4′ substituent, which projects toward the solvent and is presumably disordered. The crystallographic structure shows that CQ is bound and partially buried within the cofactor binding site of pfLDH (Figs. 4*b* and 5), occupying a position similar to that of the adenyl ring of the cofactor in the ternary complex structure (1). When overlaid on the ternary structure (Fig. 5), the quinoline ring is seen to lie in a plane similar to that of the adenyl ring but is shifted by an average translation of 2.0 Å and rotation of about 30° in this plane. This leaves the chlorine pointing toward Asp-53, and the 4′ substituent projecting toward Glu-122. The quinoline ring itself appears to be tightly bound, with average temperature factors for the ring atoms of 16.7 Å^2 compared with 11.3 Å^2 for all protein atoms. Some 471 Å^2 of solvent-accessible surface area is occluded between the bound CQ and the protein (calculated with QUANTA).

The drug makes a limited number of specific contacts with the protein (Fig. 4*b*). Most prominent is a hydrogen bond to the charged side-chain of the glutamic acid at position 122. This residue is unique to the plasmodium form of the enzyme. In all mammalian forms of LDH, and most other forms, there is a Phe in this position that is not capable of making this interaction. There are two further hydrogen bonds between CQ and the protein. The ring nitrogen is involved in a hydrogen bond network to which the side chain of Asp-53 and main chain carbonyl group and nitrogen of glycine 99 also contribute. These are both highly conserved residues found in all LDH sequences known to date and are important for cofactor binding. This suggests these contacts would not contribute any specificity for binding the malarial form of the enzyme.

Further selectivity appears to result from a series of hydrophobic interactions between the drug and enzyme. Perpendicular pi-stacking (14) between the quinoline ring system and phenylalanine side chain at position 100 provides a further interaction unique to the malarial form of the enzyme. In mammalian LDHs, the equivalent residue is always either Ala or Val, both of which are incapable of pi-stacking. This residue is at the base of the extended specificity loop, a dominant region of difference between pfLDH and all other LDH structures and

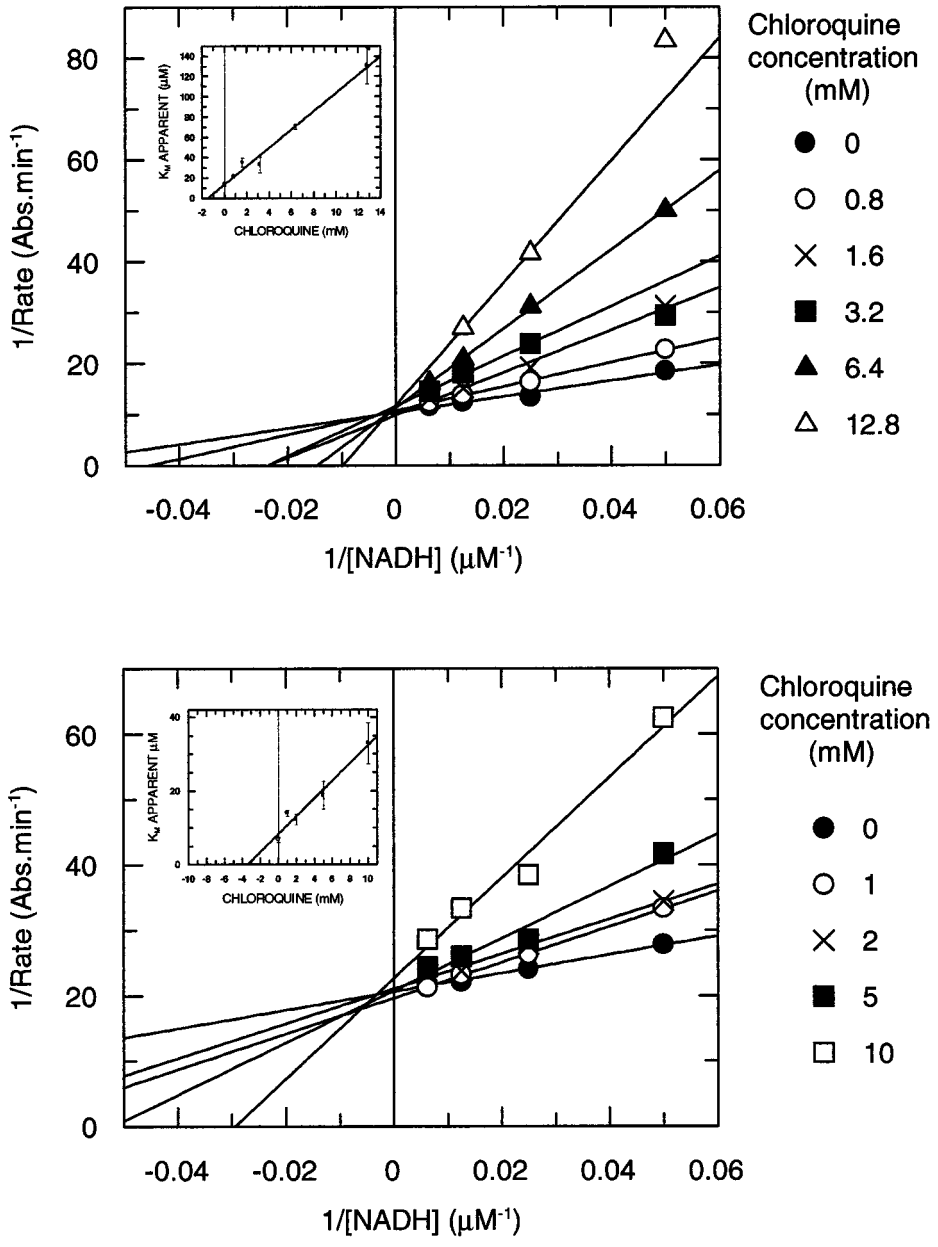

FIG. 2. **Lineweaver-Burke plot showing chloroquine is a competitive inhibitor of both pfLDH (*top*) and pig muscle LDH (*bottom*).** The apparent K_m values derived from this data are plotted against CQ concentration in the inserts. The K_i values derived from these plots are 1.3 ± 0.2 and 3.5 ± 0.3 mM for pfLDH and pig LDH, respectively.

which forms a prominent cleft alongside the active site (1). Other nearby aromatics include Phe-52 and Tyr-85, the former again unique to pfLDH.

A dominant feature in the electron density for the quinoline is the chlorine atom. When compared with the ternary complex (Fig. 3), the chlorine is seen to occupy a similar position to the N3 atom of the adenyl ring from NADH. The chlorine makes surprisingly few contacts with the protein, these being limited to van der Waals contacts with Gly-27 and Ala-98, both of which are highly conserved residues, and limited contact with Asp-53. The bulk of this predominantly hydrophobic atom may be an important factor in orienting the quinoline for binding.

The results of the inhibition studies are consistent with chloroquine being a competitive inhibitor (with respect to NADH) of the LDH enzyme activity (Fig. 2). Analysis of the data gave CQ inhibition constants (K_i) of 1.3 ± 0.2 mM with pfLDH and 3.5 ± 0.3 mM with pig muscle LDH at pH 7.0. Inhibition of pfLDH at pH 8.0 by CQ is unchanged, but the K_i rises to 5 mM at pH 6.0 (data not shown). This suggests preferential binding of the monoprotonated form of CQ over the diprotonated species.

DISCUSSION

A comparison of the apo and CQ complex structures of pfLDH shows there is very little change in the protein structure on CQ binding (Fig. 3), with the overall root mean square deviation for positions of all Cα atoms between the two structures of only 0.17 Å. The largest changes are observed in or adjacent to the CQ binding site, where the Cα of Ile-54 moves by 0.74 Å and Asp-86 Cα by 0.8 Å. Two ordered water molecules observed in the apo structure are displaced on binding of CQ. A comparison of both the apo and CQ complex structures with the ternary structure of pfLDH (1) shows more substantial rearrangements, most significantly in the extended substrate-binding loop (residues 102–108). In the absence of bound substrate and cofactor, this loop is disordered in both the apo and CQ complex structures. This has previously been noted for apo forms of other lactate dehydrogenases (15–17).

The crystal structure of the ternary complex of pfLDH +

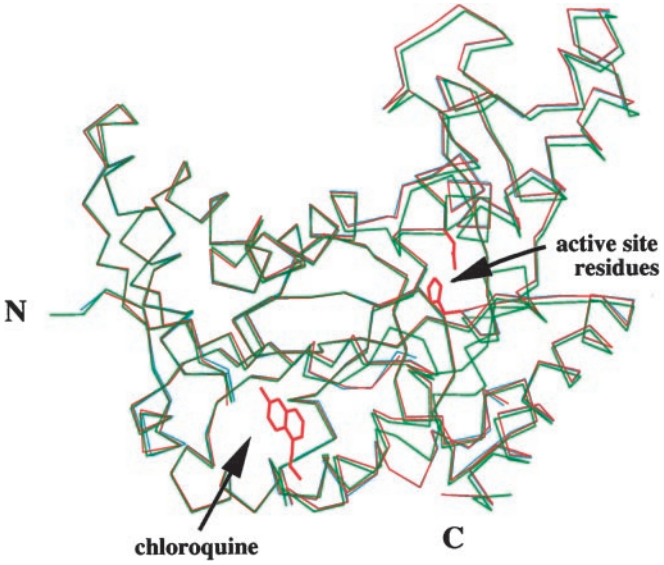

FIG. 3. **Superimposed Cα traces for apo-pfLDH (*blue*), CQ-LDH complex (*red*), and the ternary complex of pfLDH (*green*).** The bound chloroquine is also shown. Note that the specificity binding loop (residues 102–108) is disordered in both the apo and CQ complex forms and is not shown. Side chains of the active site His/Asp pair are displayed in the structure of the CQ·pfLDH complex, indicating the proximity of the CQ binding site to the active site.

NADH + oxamate (a substrate analogue) revealed an unusual association between cofactor and enzyme, evidenced by an approximately 1-Å shift in the placement of the nicotinamide group relative to other forms of LDH. This alteration is believed to be an adaptation assisting the parasite to survive in the anaerobic conditions prevalent within erythrocytes by reducing product inhibition associated with the enzyme. This movement originates from a series of amino acid changes along the cofactor binding groove but concentrated in the region occupied by the nicotinamide group. In the CQ binding region, there is only one minor change within van der Waals contact of the quinoline, Ile-54 (normally valine in mammalian LDHs). The overall retention of shape complementarity between the mammalian and malarial forms in this region is consistent with CQ also binding the mammalian form of the enzyme, albeit with lower affinity in the absence of the specific interactions with Asp-53, Phe-100, and Glu-122.

Chloroquine as an Inhibitor of pfLDH—Although in previous work (7) some evidence of CQ binding to pfLDH was reported, CQ was not found to inhibit pfLDH activity. The overlap of the CQ and NADH binding sites observed in the crystal structures suggested CQ should form a competitive inhibitor of the enzyme because the cofactor is required to bind and then be released during the catalytic cycle. This expectation was confirmed by the enzymatic activity experiments. The measured K_i values of 1.3 and 3.5 mM for inhibition of malarial and pig LDH, respectively, are high, partially explaining previous descriptions that CQ was not inhibitory. The inhibition is competitive with respect to NADH for both enzymes, as shown by the Y-axis intercepts in Fig. 2. This behavior is consistent with the crystal structure which shows a single binding site for CQ in the NADH-adenine pocket. Although it seems unlikely that inhibition at this level would provide a sufficient explanation for the effectiveness of CQ as an antimalarial, this activity might be amplified *in vivo* through the high local levels of CQ known to accumulate within the parasite (3). There is some support for this in the experiments of previous workers (6, 7) where labeled CQ analogues appear to have been sufficiently concentrated within the intracellular compartments of parasites, in infected erythrocytes, to enable isolation of CQ·pfLDH affinity labeled complexes. However, the limited affinity and selectivity of CQ for the malarial form of the enzyme suggests any biological efficacy derived through this route is likely to be supplementary to other antimalarial activities of the quinolines.

The low level of inhibition by CQ correlates with the limited interactions observed between CQ and the enzyme. It is additionally unsurprising that the selectivity for the malarial form of the enzyme is not pronounced. Despite the specific interactions described above, there remain a significant number of common structural features within the CQ binding site between the malarial and pig LDH structures. However, although the K_i values are relatively high, it is important to note that the association of CQ with the malarial form is favored by a net change in free energy equivalent to about 2 kJ/mol relative to mammalian LDH. This modest gain suggests that the quinoline template might provide a useful lead from which further specificity and binding could be developed. As glycolysis is the principle source of ATP for the parasite, which cannot undertake oxidative phosphorylation (18), disruption of the glycolytic pathway by inhibition of pfLDH appears to be an effective route for killing the parasite. The proximity of the CQ binding site to other regions of the enzyme both important for its activity and of unique structure compared with human LDH implies that the inclusion of quinoline moieties in composite compounds capable of bridging these regions might lead to dramatic additive increases in both selectivity and inhibitory activity. Parallels for the development of inhibitors to nucleotide binding sites have, for example, recently been described by Gray *et al.* (19) where a series of kinase inhibitors have been synthesized based on the binding of substituted purines to the ATP binding site of human cyclin-dependent kinase2 (CDK2).

Menting *et al.* (7) have previously reported that pfLDH is particularly sensitive to inhibition by hematin and that CQ reduces this activity by 2 orders of magnitude. Using fluorescence studies, we have been able to show hematin binds tightly to pfLDH (K_d = 0.25 μM, results not shown) but so far have been unable to produce crystals of a hematin·pfLDH complex. The modulatory effect of CQ on hematin inhibition is consistent with related binding sites for both compounds, and the CQ/hematin adduct, on the enzyme.

Conclusions—The mode of action of chloroquine and related quinolines has remained unclear despite extensive usage of these compounds as antimalarials for many years. Structural analysis of complexes of these compounds with their molecular targets could provide an invaluable boost to the design of new drugs urgently needed to overcome developing drug resistance. Previous studies (6, 7) identified pfLDH as a potential molecular target for CQ. In this study we have shown that CQ acts as a modest competitive inhibitor of the enzyme and have determined the first structure of a complex between chloroquine and an enzyme. Although we remain cautious of the importance of pfLDH inhibition in the overall efficacy of CQ, the structure of this complex demonstrates that specific targeting of this important glycolytic enzyme from the parasite should be feasible. Structure-based drug design studies incorporating this template could lead to the production of new forms of efficient pfLDH inhibitors as antimalarials.

Acknowledgments—We are grateful to Mark Banfield, for general assistance with pfLDH preparation and crystallography, and to Christopher Higham, Dilek Turgut-Balik, and John Holbrook, for access to the pfLDH clone.

JOURNAL OF RAMAN SPECTROSCOPY
J. Raman Spectrosc. 2006; **37**: 326–334
Published online in Wiley InterScience (www.interscience.wiley.com). DOI: 10.1002/jrs.1471

JRS

FT-Raman and NIR-SERS characterization of the antimalarial drugs chloroquine and mefloquine and their interaction with hematin†

S. Cîntă-Pînzaru,[1] N. Peica,[2] B. Küstner,[2] S. Schlücker,[2] M. Schmitt,[3] T. Frosch,[3] J. H. Faber,[4] G. Bringmann[4] and J. Popp[3]*

[1] Molecular Spectroscopy Department, Babes-Bolyai University, Kogălniceanu 1, RO-400084 Cluj-Napoca, Romania
[2] Institut für Physikalische Chemie, Universität Würzburg, Am Hubland, D-97074 Würzburg, Germany
[3] Institut für Physikalische Chemie, Universität Jena, Helmholtzweg 4, D-07743 Jena, Germany
[4] Institut für Organische Chemie, Universität Würzburg, Am Hubland, D-97074 Würzburg, Germany

Received 16 June 2005; Accepted 1 September 2005

Raman and surface-enhanced Raman scattering (SERS) spectroscopies were employed to probe the interaction of the antimalarial drugs chloroquine (CQ) and mefloquine (MQ) with hematin. NIR-SERS spectra of both quinoline derivatives were obtained from a colloidal gold surface. Strong chemical interactions of each drug with the Au particles are observed and the similarities of the two NIR-SERS spectra allowed to predict a similar orientation geometry for both of the drugs on the colloidal surface, namely through the quinoline skeletal part of each molecular structure.

Separately, the adsorption behavior of hematin on the Au colloid was studied under nonresonant conditions. In addition, both hematin–antimalarial drug systems (CQ and MQ) were prepared and investigated by NIR-SERS.

KEYWORDS: antimalarials; hematin; NIR-SERS

INTRODUCTION

Malaria is a global tropical disease with about 3 million deaths per year.[1,2] Owing to the increasing number of resistant strains of *Plasmodium falciparum*, new antimalarial drugs, among them quinoline derivatives, are needed. For therapeutic treatments, the free heme released in the parasite food vacuole is considered as an attractive pharmacological target: it is the most specific target that can be utilized since it comes from the hemoglobin digestion by the parasite in infected erythrocytes.[3] As the precise mechanisms of both heme aggregation and quinoline transport, are not exactly known many of quinoline-based compounds have been investigated. However, precise structure–activity relationships for optimal antimalarial activity remain unclear.[4] The difficulty in determining exact structure–function relationships arises from the dual requirements that heme polymerization inhibitors not only disrupt the process of hemozoin formation but also concentrate within the digestive vacuole of the parasite, which is the site of heme aggregation.[4]

In spite of the huge amount of available pharmaceutical and medical data related to the antimalarials and their possible inhibition effects,[1–13] only few vibrational spectroscopic characterizations of several quinoline derivatives[14–17] and, recently, of hematin[18–20] have been published. The hematin–chloroquine CQ mechanism interaction was recently reported using resonance Raman (RR) spectroscopy.[18] Polarization-resolved RR spectra of hematin and its complex with CQ were recorded under Q-band resonance conditions in order to monitor the binding of the drug to the heme structure. A noncovalent interaction in the electronic ground state of the CQ–heme complex was concluded.[18]

Surface-enhanced Raman scattering (SERS) has been proven to trigger exciting opportunities in the field of biomedical spectroscopy,[21,22] where it allows the study of structural–functional properties of biologically relevant molecules, which are often present in extremely small concentrations at physiological level. SERS combines the

†Presented as part of a commemorative issue for Wolfgang Kiefer on the occasion of his 65th birthday.

*Correspondence to: J. Popp, Institut für Physikalische Chemie, Universität Jena, Helmholtzweg 4, D-07743 Jena, Germany.
E-mail: Juergen.popp@uni-jena.de
Contract/grant sponsor: Deutsche Forschungsgemeinschaft.
Contract/grant sponsor: Fonds der Chemischen Industrie.

structural information available by Raman spectroscopy with ultrasensitive detection limits, allowing a detection down to the single-molecule level.[21]

In particular, SERS with colloidal gold nanoparticles is attractive for biomedical applications.[23] It was shown[23] that gold nanostructures have comparably good SERS enhancement factors as silver structures when near-infrared excitation is applied. The uniform size distribution, the chemical stability, and the optical properties of the Au colloidal surface provide important advantages in performing SERS experiments with light-sensitive molecules.

RR data[18,19] of hematin and the hematin–CQ complex[18] have been recently published, but, to the best of our knowledge, SERS investigations of the antimalarial drugs or of the monomeric precursor, hematin, have not been reported.

When RR spectroscopy is employed to investigate the chromophore-containing species in the presence of a drug, the available information is selectively related to the structure of chromophore and its possible perturbation caused by the drug. When the drug targets the nonchromophore part of the macromolecular structure, this information is unavailable using RR spectroscopy. In order to overcome this disadvantage, the use of SERS spectroscopy is the proper alternative, providing information about the adsorbed molecular species,[14,17,22] their functional groups involved in adsorption, the influence of the environmental pH conditions on adsorption, interaction between a specific drug and the target molecule upon adsorption on a proper surface, the mechanisms at the interface, etc.

Here, we employed NIR-SERS in order to monitor the interaction of hematin with two widely used antimalarial drugs, CQ diphosphate ($C_{18}H_{26}ClN_3{}^*2H_3PO_4$, 7-chloro-4(4-diethylamino-1-methylbutylamino)-quinoline diorthophosphate, CQ) and mefloquine MQ hydrochloride (2-piperidinil-2,8-bis(trifluoromethyl)-4-quinolinemethanol hydrochloride, MQ).

EXPERIMENTAL

Chemicals

The gold colloid was prepared according to the method reported by Sutherland and Winefordner.[24] Briefly, 40 ml of distilled water was added to 0.1 ml of 4% (w/v) $HAuCl_4$ with stirring, then 1 ml of 1% (w/v) trisodiumcitrate dihydrate solution was added drop wise, and the resulting mixture was boiled for 5 min without stirring. At the end of boiling, the color was intensive magenta-red.

The hematin–MQ mixture (molar ratio 1:1) was prepared by addition of the 0.1 ml 25×10^{-3} M of hematin to 2.5 ml of 10^{-3} M MQ solution; for hematin stabilization, 3 µl 10^{-1} M NaOH and 1 µl 10^{-1} M HCl solutions were added. The hematin–CQ complex (molar ratio 1:1) was prepared by the 0.2 ml of 25×10^{-3} M of hematin with 0.125 ml of 4×10^{-2} M of CQ solution, and 1 µl of 10^{-1} M NaOH solution for hematin stabilization.

The MQ and CQ solutions used for SERS samples preparation were 10^{-2} M and 4×10^{-2} M respectively. The SERS samples were prepared by adding 2 µl of each mixture to 2 ml gold colloid. The final concentrations of the SERS samples were 0.9×10^{-5} M for MQ, 3.9×10^{-5} M for CQ, 2×10^{-5} M for hematin, 0.9×10^{-6} M for hematin–MQ (1:1 molar ratio), and 1.5×10^{-5} M for hematin–CQ (1:1 molar ratio).

Apparatus

A UV-VIS-NIR Perkin–Elmer Lambda 19 spectrophotometer with a scan speed of 240 nm min^{-1} was used for recording the absorption spectra of the samples.

The FT-Raman spectra were obtained with a Bruker IFS 120 HR spectrometer with an integrated FRA 106 Raman module and a resolution of 1 cm^{-1}. The 1064-nm radiation from an Nd-YAG laser with an output of 400 mW was employed for the excitation. A Ge detector operating at liquid nitrogen temperature was used.

The SERS spectra on Au colloid were recorded with a Dilor Labram spectrometer using the 785-nm excitation line from an NIR diode laser. The spectra were collected in the backscattering geometry using a microscope equipped with an Olympus LMPlanFL 10× objective. The spectral resolution was 4 cm^{-1}. The detection of a Raman signal was carried out with a CCD camera (Photometric model 9000) and for the signal acquisition the analyzing software package LabSpec 3.1 was employed. The laser output power was 200 mW. The SERS spectra were obtained by averaging 10 cycles of 20 s. Each experiment was run three times giving a very good reproducibility.

RESULTS AND DISCUSSIONS

FT-Raman spectra of the solid polycrystalline CQ and MQ species are presented in Fig. 1 with the corresponding insertion of the molecular structure.

Electronic absorption spectra

The gold colloid displays characteristic optical properties, which have to be considered under the point of view of the electromagnetic mechanism,[25–27] associated with the SERS effect. The absorption spectra of the pure gold colloid and the drug–colloid system for both antimalarial drugs are presented in Figs 2 and 3 respectively. The absorption bands of the colloids are due to plasmon excitation. The pure colloids show a plasmon resonance at ~534 nm. Upon addition of the drug solution, in both cases a red-shifted new band was observed at about 791 nm, indicating an aggregation of the Au particles in the presence of the drug. This result suggests the possibility of using the NIR-SERS excitation of the surface plasmon resonance of the aggregated particles in the presence of the respective drug.

JRS

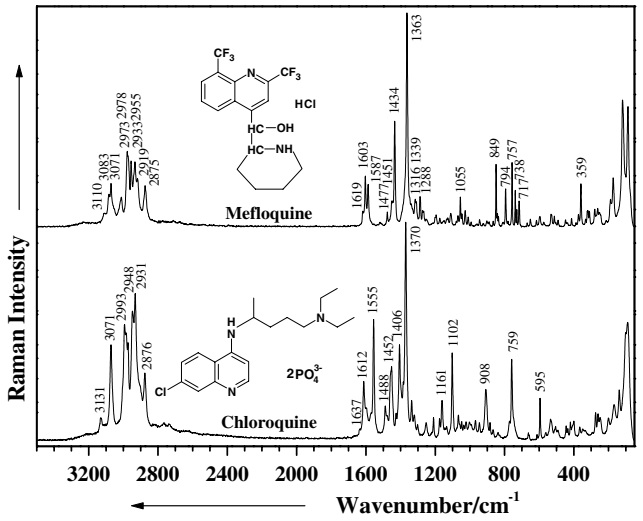

Figure 1. FT-Raman spectra of chloroquine diphosphate and mefloquine hydrochloride. The molecular structure of each drug is inserted.

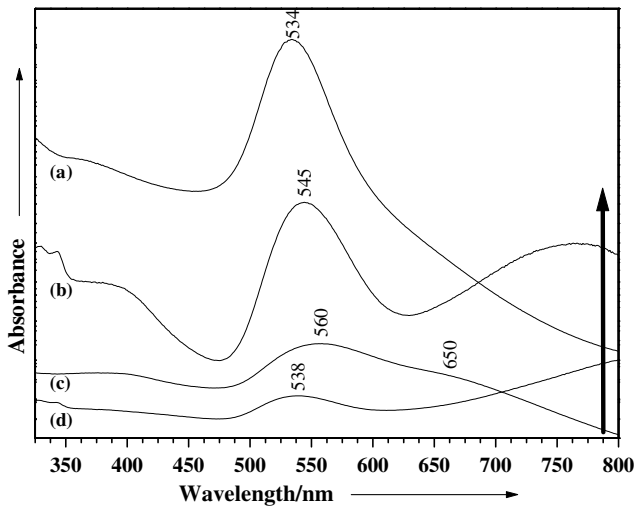

Figure 2. Absorption spectra of the gold colloid (Au) (a), hematin–CQ–Au (b), hematin–Au (c), and CQ–Au (d). The arrow indicates the excitation wavelength employed for NIR-SERS.

Upon addition of hematin to the Au colloid, a decrease and broadening of the absorption band was observed with a new developed band at about 650 nm having a tendency to NIR shifting (Fig. 2(c)). This fact further supports motivation for NIR-SERS investigations on hematin species.

The hematin–CQ and hematin–MQ systems (1 : 1 molar ratios), however, exhibit different absorption patterns upon addition into the Au colloid (Figs 2(b) and 3(b) respectively). In the case of hematin–CQ, the new band at 760 nm was well defined, whereas in the case of hematin–MQ, this new expected band had only a tendency to slowly develop,

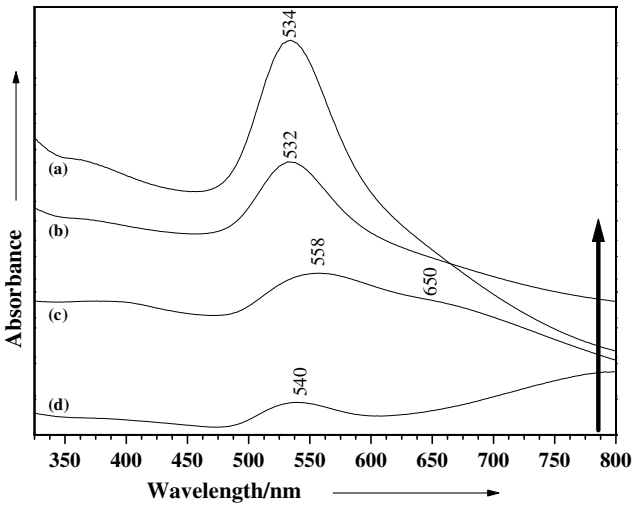

Figure 3. Absorption spectra of the gold colloid (Au) (a), hematin–MQ–Au (b), hematin–Au (c), and MQ–Au (d). The arrow indicates the excitation wavelength employed for NIR-SERS.

indicating a smaller degree of particle aggregation in the presence of the molecular species than anticipated.

NIR-SERS spectra

The recorded spectra of CQ, hematin, and CQ–hematin (1 : 1 molar ratio) are presented in Fig. 4 and those of MQ and MQ–hematin system in Fig. 5, respectively.

CQ and MQ on gold colloid

The collected vibrational FT-Raman and NIR-SERS data of the two drug species are summarized in Tables 1 and 2 respectively. The proposed assignments[28] are based on the

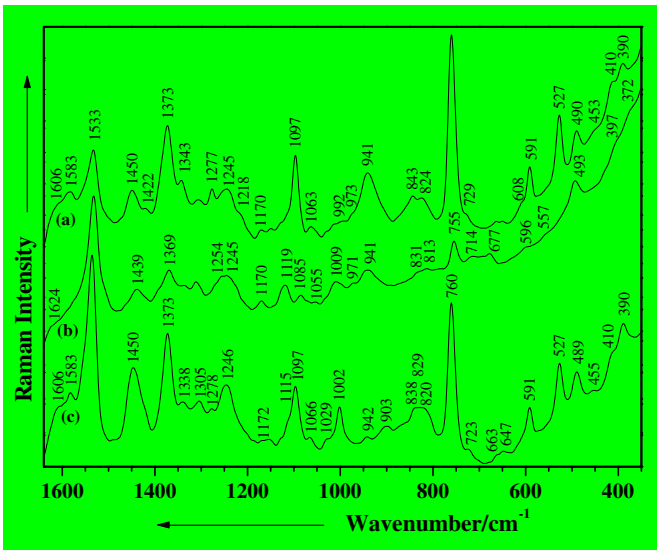

Figure 4. NIR-SERS spectra of CQ–hematin system (a), hematin (b), and CQ (c) on gold colloid. Excitation: 785 nm, 30 mW.

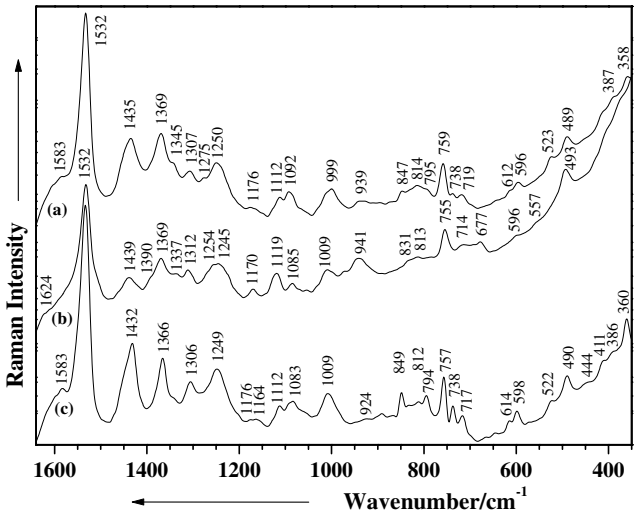

Figure 5. NIR-SERS spectra of MQ–hematin system (a), hematin (b), and MQ (c) on gold colloid. Excitation: 785 nm, 30 mW.

Table 1. Vibrational FT-Raman and NIR-SERS data (cm^{-1}) of chloroquine diphosphate (CQ) and their assignments

FT-Raman (cm^{-1})	NIR-SERS Au colloid (cm^{-1})	Vibrational assignment
3131 w	–	ν_{as}(N–H)
3071 s	–	ν_s(N–H)
2993 s	–	ν_{as}(C–H) aromatic
2984 s	–	ν_s(C–H) aromatic
2973 s	–	ν_s(C–H)
2948 s	2944 m	$\nu_{as}(CH_3)$
2931 s	–	$\nu_{as}(CH_2)$
2903 sh	–	$\nu_s(CH_2)$
2876 m	2859 m	$\nu_s(CH_3)$
1637 w	–	Δ(N–H) amine
1612 ms	1606 sh	ν(C═N), δ(N–H)
1598 sh	1583 m	ν quin. ring
1571 sh	–	ν(CCC), ν(C═N ring)
1555 s	1533 vs	ν(C═N ring)
1488 wm	1492 w	ν(C–C)ring, νC_2H_5
1476 sh	–	ν(C–C) ring
1452 ms	1450 ms	ν(C–C), δ(C–H), ν_{as}(-CH_3 + CH_2) aliphatic
1426 w	–	ν(C–C), δ(C–H) ring
1406 s	–	ν(C–C), δ(C–H) ring
1385 m	–	ν(C–C) benzene ring
1370 vvs	1373 s	ν(CCC) quin. + ν_s(C–CH_3) aliphatic
1336 wm	1338 m	ν(C–C), δ(C–H) ring
1321 w	–	ν(C–C)
1302 w	1305 m	ip δ(C–H), amine

Table 1. (*Continued*)

FT-Raman (cm^{-1})	NIR-SERS Au colloid (cm^{-1})	Vibrational assignment
	1278 m	ν(C–N)
1253 w	1246 m	ν(C–C)quin., ν(C–N)amine
1210 w	1212 sh	ν(C–CH_3), ν tertiary diethyl amine
1175 w	1172 w	ν(C–C)
1161 wm	1157 w	ν(C–C), secondary aliphatic amine
1144 w	–	ν quin. ring
1135 w	1128 sh	ν quin. ring
1102 s	1097 m	ν(Cl-quin.)
1066 w	1066 w	ν(P═O)
1048 sh	–	$\nu(PO_4^{3-})$
1036 w	–	pyr. trigonal stretch
1023 w	1029 sh	ν(P–O)
1003 w	1002 m	ν quin
991 sh	–	pyr. ring breath
968 w	–	ν benz., op δ(C–H), C-dialkylamine
945 w	942 w	ν(C–C)
908 m	903 wm	op δ(C–H)
884 w	–	op δ(C–H) ring + aliphatic
867 w	–	ν(C–N–C), op δ(C–H)
837 w	838 m	op δ(C–H)
827 w	829 m	ν_{as}(C–N)
801 vw	–	op δ(C–H)
771 sh	–	T (C–H) quin.
759 s	760 s	Δ(N–H) amine, CH_3 + ip ring def
745 sh	723 sh	ν(C–Cl), op δ(N–H)
663 vw	663 vw	Δ(quin. –Cl), τ(C–H) quin.
658 vw	647 vw	T (C–H) quin.
613 vw	–	Δ(C–H), δ amine
595 m	591 m	Δ(quin., C–Cl)
562 vw	–	op δ(C–C), (C–H)
535 w	527 m	op δ(C–N–C)
505 w	–	op δ(CCN)
492 vw	489 m	op δ quin., δ secondary aliphatic amine
434 w	390 m	–
255 w	–	Δ(O–P–O)
–	252 vvs	Au–N
249 w	–	T (C–H) quin.
201 w	–	T and δ quin.
168 wm	–	Lattice vibrations
137 m	–	Lattice vibrations
99 s	–	Lattice vibrations
88 s	–	Lattice vibrations

s, strong; m, medium; w, weak; v, very; sh, shoulder; ν, stretching; δ, bending; τ, torsion; ip, in-plane; op, out-of-plane; pyr., pyridine moiety; quin., quinoline ring.

Table 2. Vibrational FT-Raman and NIR-SERS data (cm^{-1}) of mefloquine hydrochloride (MQ) and their assignments

FT-Raman (cm^{-1})	NIR-SERS Au colloid (cm^{-1})	Vibrational assignment
3110 w	–	ν_{as}(N–H)
3083 m	–	ν_s(C–H)
3071 m	–	ν_s(C–H) aromatic
3011 m	–	ν_s(C–H)
2978 ms	–	ν(CH, CH_2)
2973 sh	–	ν(CH)
2955 ms	–	ν_{as}(CH)
2933 ms	–	ν_{as}(CH_2)
2918 m	2920 m	ν_s(CH_2)
2875 m	2870 m	ν_s(CH) bridge
1619 w	–	δ(N–H), ν(C=C)
1603 ms	–	ν quin. ring
1587 m	1583 m	ν(C=C)
1555 vw	1532 vs	ν(C=N), ν(C=C)
–	–	ν(C–C) ring
1477 w	–	ν(C–C) ring
1451 w	–	ν (C=N), ν(C–C)
1434 s	1432 m	ν(C–C), δ(C–H) ring
–	–	ν(C–C) adsorbed quin. ring
1363 vvs	1366 m	ν(CCC) quin.
1339 w	1343 sh	δ(C–H) ring + ν(CF)
1316 w	–	ν(-CF_3)
–	1306 m	ip δ(C–H)
1288 wm	–	ν(C–N), ν(-CF_3)
1253 w	1249 m	ν C–C) quin., ν(C–N)amine
1195 w	–	ν(C–O)
1174 w	1176 w	ν(C–C), ν(N–H)
1149 vw	1164 w	ν(C–C), δ(C–H)
–	–	ν quin. ring
1111 w	1112 w	ν quin., ν(-C–F)
1069 w	1083 wm	ν quin.
1055 wm	–	ν piperidine ring
1046 w	–	ip δ(C–H)
1027 w	–	pyr. trigonal stretch
1010 w	1009 m	ν quin.
993 vw	–	ν pyr. (breath)
960 vw	–	ν(C–C)
944 vw	–	δ(C–C–OH)
903 vw	–	ν(C–C)
889 vw	891 w	γ(O–H)
866 vw	867 w	ν(C–N–C) piperidine
849 ms	849 w	ip δ(C–H) + piperidine breathing
835 w	833 w	ip δ(C–H) + piperidine stretch
808 vw	812 w	op δ(C–H)
794 m	–	op δ(C–H)
757 ms	–	γ[(N–H), CH] + ip ring def.
738 m	717 wm	op δ(C–H)
729 wm	–	δ(C–F), op δ(C–H)
717 wm	–	δ(CF_3), op δ(C–H)
670 w	665 w	τ(C–H) quin.
651 w	645 w	τ(C–H) quin.
616 w	614 w	δ(quin. +CF_3)
595 w	598 wm	ip δ(CNC), δ(OH)
532 w	522 w	op δ(C–C), (C–H)
492 w	490 m	op δ(CH), γ(OH)
359 m	360 m	δ quin.
–	250 vvs	Au–N
188 w	–	τ(C–H) quin.
173 wm	–	$\tau + \delta$ quin., lattice vibrations

s, strong; m, medium; w, weak; v, very; sh, shoulder; ν, stretching; δ, bending; τ, torsion; ip, in-plane; op, out-of-plane; pyr., pyridine moiety; quin., quinoline ring.

recently reported theoretical DFT calculations of several quinoline derivatives.[14–16]

The well-known possibilities of adsorption on a metal surface, namely, physisorption and chemisorption,[25–27] support the explanation of the electromagnetic mechanism of enhancement. In the case of physisorbed species, the Raman and SERS spectra are similar in relative intensities and band positions. Additionally, when the CT (chemical enhancement) mechanism contributes to the total enhancement, the resulting SERS spectra are completely different from the corresponding normal Raman spectra.

Comparing the NIR-SERS spectra with the Raman spectra of the two individual drugs, one can notice large differences in the relative intensities and band positions, which can be explained in terms of strong chemical interaction between the molecule and the Au nanoparticles. Taking into account the information from the electronic spectra, one can conclude the formation of a CQ–Au SERS complex, where the charge transfer (CT) between the electron density of the surface plasmon and those of the molecule takes place. The 785-nm line employed for excitation of the SERS spectra matches exactly the resonance condition for this CT band. Theoretically, the CQ species could be chemisorbed through the lone pairs of each of the N atoms, of the Cl atom, or through the π-ring system. According to the surface selection rules,[26,29] the vibrational modes that have the polarizability tensor component perpendicular with respect to the surface will be predominantly enhanced, whereas those having large tensor components parallel to the surface will result in weak SERS bands. Moreover, for molecules with a planar structure, the orientation geometry at the surface could be predicted from the relative intensity of the in-plane and out-off-plane

C–H modes.[30] In the case of adsorption through the π-ring system, a characteristic red shift of the SERS bands together with their broadening on passing from Raman to SERS is usually observed.

Analyzing the NIR-SERS spectrum of CQ (Fig. 4(c)), the strongest band at 1533 cm^{-1} has the corresponding Raman band at 1555 cm^{-1} (Fig. 1, Table 1), which was assigned to the C═N stretching mode of the ring. Significant red shift from the Raman position was observed for the most representative quinoline ring-stretching modes present in the SERS spectrum (Table 1). A blue shift of the enhanced vibrational modes, as expected of a supposed N-adsorption, was not observed; therefore, a perpendicular staking of the skeletal molecular plane with respect to the surface would be less probable. One significant band at 1373 cm^{-1} (ring-stretching mode) from the NIR-SERS spectrum, however, was blue shifted with 3 cm^{-1} from its corresponding normal Raman position, which did suggest a quinoline N-adsorption. A tilted orientation of the skeletal ring would explain the decrease in the relative intensity of the SERS mode at 1373 cm^{-1} in comparison to FT-Raman (Table 1). Adsorption through one or both of the N atoms from the dialkylamine substitute was not consistent since the corresponding modes are less representative in the SERS spectrum.

In the low-wavenumber spectral range (Fig. 6(a)), a huge and broad SERS band located at 252 cm^{-1} was observed. This band is usually assigned to the Au–N and Au–Cl (when the Cl^- ions are present) stretching modes.

Taking into account these considerations, the results suggest a flat rather than tilted orientation of the quinoline ring to the Au surface, where the N ring could be close enough for a CT mechanism.

In the case of MQ, remarkable similarity with CQ in the SERS behavior has been observed, suggesting that the common skeletal structure is located in the close vicinity of the Au colloidal surface. The very strong band at 1532 cm^{-1} similar to CQ, along with the representative enhanced modes at 1583, 1432, 1366, 1249, 1009, 757, 490, 360, and 250 cm^{-1} are present (Fig. 5, Table 2). The red-shift character of the most prominent skeletal stretching modes, except for the 3 cm^{-1} blue shift of the band at 1366 cm^{-1}, the less significant piperidine moiety modes enhancement, and the presence of the band at 250 cm^{-1} suggest a tilted to flat orientation of the quinoline ring with respect to the Au surface with an N-adsorption conditioned by the steric configuration of the two trifluoromethyl substituents of the MQ skeletal ring.

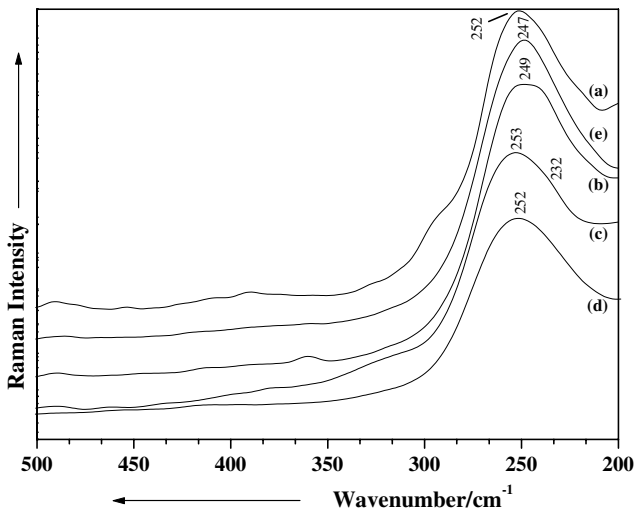

Figure 6. Low-wavenumber region of the NIR-SERS spectra of CQ (a), MQ (b), hematin (c), hematin–CQ (d), and hematin–MQ (e).

NIR-SERS spectrum of hematin

The observed vibrational Raman and NIR-SERS data of hematin adsorbed on Au colloid are summarized in Table 3, together with the proposed assignments.[18,19,31–33] In the NIR-SERS spectrum, the dominant band is located at 1532 cm^{-1}, whereas the totally symmetric stretching modes are less enhanced (Table 3). For the nontotally symmetric modes, appreciable SERS enhancements are observed.

The characteristic vibrational feature in the spin state region (1650–1500 cm^{-1}) of hematin could also reflect the dynamics of the porphyrin perturbation under different excitation energies of the laser lines, together with the change in the hematin orientation on the surfaces.

The hematin molecule on the Au surface will experience an enhanced electric field from the metal in addition to the electric field from the incident light, thus will scatter light with an enhanced intensity compared to an isolated molecule. This contribution to SERS does not require direct bonding between the adsorbate and the metal surface; increased sensitivity was recorded up to a distance of 40 Å from the metal surface. In the charge-transfer mechanism, the enhancement effect is dependent on the nature of the molecules involved. It includes transfer of charge from the metal surface through a bond. The enhancement mechanism requires new electronic transitions between adsorbate and metal (absorption band at 650 nm), made possible when hematin is at the surface. This mechanism accounts for the high specificity of SERS to the first layer of adsorbed molecules.

Owing to the NIR excitation, which is preresonant to a weak absorption band of hematin[19] but resonant to surface plasmons, RR scattering from the heme is considered to be negligible.

Preresonance still gives selectivity or sensitivity for the species containing the chromophore, but the scattering intensities are dependent on the molecular orientation at the surface, providing more information on the nature of the bonding.

In previous investigations, surface-enhanced resonance Raman scattering (SERRS) has also been used to investigate

Table 3. Raman and NIR-SERS data of hematin (cm^{-1}) for the 785-nm excitation line

NIR-SERS Au colloid (cm^{-1})	Raman[ref] (cm^{-1})	Vibrational assignment[ref]
1624 sh	1626 s	ν_{10} B_{1g} (C_aC_m)
–	1591 sh	ν_{37} E_u (C_bC_b)
–	1571 s	ν_2 A_{1g} (C_bC_b) + ν_{19} A_{2g} (C_aC_m)
–	1553 s	ν_{11} B_{1g} (C_bC_b)
1532 vs	1533 sh	ν_{38} E_u (C_aC_m)
–	1491	ν_3 A_{1g}(C_aC_m)
–	1453	ν_{28} B_{2g} (C_aC_m)
1439 w	1435	δ_s (=CH_2) (1)
1390 sh	1404	ν_{29} B_{2g} (C_aC_b)
1369 m	1373 s	ν_4 A_{1g}(C_aN)
1337 w	1340	δ_s (=CH_2) (2)
1312 wm	1309 w	ν_{21} A_{2g} δ(C_mH), δ_s(CH=)
1254 m	1260 m	ν_4, ν_9 A_{1g}
1245 m	–	?
–	1228	ν_{13} B_{1g}
1170 w	1170 w	ν_{30} B_{2g}
1119 m	1127 ms	ν_{22} A_{2g} (C_aN)
1085 w	1089	δ_{as} (=CH_2)
1055 w	–	?
1009 m	1008 w	γ(CH=)
971 w	–	?
941 m	–	?
831 w	–	?
813 w	806 wm	ν_6 A_{1g} δ($C_aC_mC_a$)
755 ms	756 ms	ν_{33}, ν_{34} A_{1g}
714 w	722	ν_{16} B_{1g} δ(C_aNC_a)
677 w	675 w	ν_7 A_{1g} δ(C_bC_aN)
596 w	–	?
557 w	555	$\nu_{49}\delta$($C_aC_bC_b$)
493 w	492	pyr. fold?
387 sh	–	?
358 sh	–	?
251 vvs	–	Au–O
232 sh	–	Au–N

w, weak; m, medium; s, strong; sh, shoulder; op, out-of-plane; ν_2–ν_7, skeletal modes of porphyrine ring; pyr., pyridine moiety; ref, 18–20,33. C_a, carbon atoms bonded to N; C_m, 'middle' carbon (N–Ca–Cm–Ca–N); C_b, the other carbons from porphyrine ring. Assignment follows the assumed D_{4h} symmetry for metallo-porphyrins.[33]

biological molecules;[22,31,32,34] for example, studies of enzymes on proteins are well known. As an example of a heme-protein, cytochrome c adsorbed on silver colloid was reported.[34] The intense bands in the spectra correspond to those found in resonance, but the relative intensities do vary when compared to resonance. It was shown[34] that the band at 1375 cm^{-1} (ν_4) is a marker for the oxidation state. By gradually titrating cytochrome c into a silver colloid, adsorption layers on the surface have been built up from below to above monolayer coverage. When this occurs, there is a relative intensity change in a number of the bands. Specifically, the ratio of the intensity of the band at 1375 cm^{-1} (A_{1g}, ν_4) relative to that at 1640 cm^{-1} (B_{1g}, ν_{10}) changes. By plotting this intensity, the formation of the monolayer could be monitored.[34] The reason for this change is that SER(R)S provided the effect, contains an appreciable SERS contribution, depends on selection rules related to those from SERS alone. Thus, as the monolayer builds up on the surface, the protein packs and the orientation of the heme in the protein relative to the surface changes. This change is reflected in the relative intensity changes between ν_4 and ν_{10}. In fact, at close-to-monolayer coverage, more subtle reorganization of the layer occurred.

Taking into account these considerations, at our concentration values of about 10^{-5} mol^{-1}, in the case of hematin, the marker band for the oxidation state is located at 1369 cm^{-1} (Fig. 4(b)). The band at 1533 cm^{-1} is believed to correlate with the porphyrin core size.[31] The slight decrease in its wavenumber on passing from Raman to SERS (Table 3) implies an expansion of the porphyrin ring, a plausible consequence of the increased interactions between the pyrrole nitrogen atoms and the metal surface. The possibility that the hematin adopts a denatured geometry upon chemisorption and that the heme group is situated in a smaller gap within the aggregates cannot be excluded.

A nonbonded interaction between the pyrrole N atoms and a presumable drug species would affect the position of this band in the SERS spectra of the hematin–drug complexes.

SERS of hematin–drug systems

Individually, considering hematin in the presence of CQ, the NIR-SERS spectrum of hematin is affected in relative intensities and positions of several bands. The NIR-SERS spectrum of hematin–CQ system is more similar to those of the CQ except for the dominance of the band at 760 cm^{-1}, which becomes the strongest one (Fig. 4(a)). This fact could also suggest a preference of CQ adsorption instead of hematin on the Au particles. Such a coverage effect of the active sites of metal only with the CQ species would not allow to observe contributions from hematin raised above.

Several differences in the band positions or relative intensities of the NIR-SERS bands of the complexes, compared to those from the NIR-SERS of the pure hematin or each pure drug, allowed the presumption of an interaction evidence between the drug and the hematin.

Following the metallo-porphyrin ring modes of the hematin in the presence of CQ antimalarial drug under the surface plasmon resonance, the band at 1373 cm^{-1} (shifted from 1369 cm^{-1} in the SERS of pure hematin) increases in relative intensity, but dramatically overlaps with the CQ contribution. The position of the band at 1533 cm^{-1} was

found to be unaffected, suggesting that the pyrrole N atoms of the porphyrin macrocycle are not involved in a possible interaction with the drug. A significant increase in the relative intensity of the band located at 941 cm^{-1} (porphyrin skeletal mode) was observed. Therefore, the hypothesis of CQ adsorption as the first monolayer up to the coverage effect of the active metal sites could be excluded. The relative intensities of the bands attributable to the adsorbed CQ are different in the case of the hematin–CQ system, indicating changes in the attached geometry of CQ when the hematin coexists.

More probably, the heme core upon adsorption becomes sensitive to the presence of CQ as an axial π acceptor ligand (the wavenumber increased from 1369 to 1373 cm^{-1}). This hypothesis would also explain the enhancement of the porphyrin mode at 941 cm^{-1}.

In the low-wavenumber spectral range, the band shape (Fig. 6(d)) attributable to the molecule–Au bond is different from that of the individual species (pure hematin or CQ). This fact further supports the presumable interaction of the hematin and CQ species upon adsorption.

The contribution of the CQ aliphatic chain was not observed in the spectrum of the hematin–CQ system, suggesting that this moiety of CQ is not involved into the interaction of the two species. The involvement into this possible interaction is more predictable for the quinoline ring.

The hematin–MQ system adsorbed on Au particles displays specific SERS changes in the relative intensities and band positions compared with those of either hematin–Au or MQ–Au SERS systems. The strongest band at 1532 cm^{-1} being characteristic for both species, remains unshifted, whereas the marker band at 1369 cm^{-1} of hematin is significantly increased relative to that at 759 cm^{-1} (Fig. 5(a)). Small increases by 2–3 cm^{-1} of the modes mostly associated to the quinoline stretching were also observed. These modifications could be explained as in the case of the CQ–hematin system, in terms of individual adsorption of each species through the chemisorption mechanism, where the first monolayer could contain both MQ and hematin, or interaction between the two species upon adsorption. Taking a closer inspection of the band positions, the small shifts and relative intensities modification observed in the band positions of the MQ–hematin system suggest that an individual adsorption or physical coexistence of the two species would be less probable. A perturbed geometry upon coadsorption resulting from their interaction would be responsible for this spectral change. Therefore, the SERS data rather support an interaction between the hematin and MQ upon adsorption on Au particles, where the pyrimidine moiety of MQ is less involved. However, it would be speculative to predict the interaction geometry at this point. Further experimental SERS data on these compounds at the physiological pH values of the infected erythrocytes are certainly necessary to get more insight into the physical chemistry of antimalarial complex mechanisms.

As resumed by Pagola *et al*,[6] their previous studies have established that the quinoline antimalarial drugs are associated with the detoxication of hemozoin by crystallization; therefore, their therapeutic effect occurs by interference with the formation of that solid phase. The proposed mechanisms for such a drug action were classified into three categories: (1) direct binding of the drug to heme monomers or dimers in solution, which interferes with the crystallization of hemozoin; (2) enzymatic inhibition of a protein that catalyses hemozoin crystallization, and (3) chemisorption of the drug onto crystallized hemozoin, leading to inhibition of further heme aggregation.

From the above presented results, the first point raised by Pagola *et al*.[6] was investigated in depth using surface-enhanced Raman spectroscopy. Since the micro-Raman spectra of hemozoin encapsulated within the food vacuole of a *P. falciparum* infected erythrocyte and of hematin were found to be identical,[20] and the band at 1374 cm^{-1} assigned to A_{1g} modes observed upon 780-nm line excitation was used for Raman imaging of hemozoin within its natural environment,[20] the present NIR-SERS results open the possibility to further investigate the hematin-drug systems *in vivo*.

CONCLUSIONS

FT-Raman and NIR-SERS spectra of chloroquine diphosphate and MQ hydrochloride were recorded and discussed.

The first NIR-SERS spectroscopic investigation of hematin in the presence of two widely used antimalarial drugs is reported. The modifications in the spectra of each of the hematin–drug systems could be explained in terms of interaction between the two species, where the aliphatic chain of CQ, or the pyrimidine moiety in the case of MQ, were less involved into interaction upon adsorption on Au particles. The heme core was supposed to become sensitive to the presence of the respective quinoline skeletal ring as an axial ligand upon adsorption on the metal particles.

The present results strongly motivate further NIR-SERS investigations in order to get more insight into the *in vivo* mechanisms of malaria pigment–drug interaction and resistance.

Acknowledgements

We gratefully acknowledge financial support from the Deutsche Forschungsgemeinschaft (Sonderforschungsbereich 630 ''Recognition, Preparation, and Functional Analysis of Agents Against Infectious Diseases'', projects C1 and A2), and from the Fonds der Chemischen Industrie.

REFERENCES

1. Stevenson MM, Riley EM. *Nat. Rev. Immunol.* 2004; **4**: 169.
2. Reinaldo TD, Osvaldo AS-F, José F-VD. *J. Braz. Chem. Soc.* 2002; **13**: 727.

3. Robert A, Benoit-Vical F, Dechy-Cabaret O, Meunier B. *Pure Appl. Chem.* 2001; **73**: 1173.
4. Ziegler J, Linck R, Wright DW. *Curr. Med. Chem.* 2001; **8**: 171.
5. Monti D, Vodopivec B, Basilico N, Olliaro P, Taramelli D. *Biochemistry* 1999; **38**: 8858.
6. Pagola S, Stephens PW, Bohle DS, Kosar AD, Madsen SK. *Nature* 2000; **404**: 307.
7. Ridley RG. *Nature* 2002; **415**: 686.
8. Olliaro P. *Pharmacol. Ther.* 2001; **89**: 207.
9. Foley M, Tilley L. *Pharmacol. Ther.* 1988; **79**: 55.
10. Vippagunta SR, Dorn A, Ridley RG, Vennerstrom JL. *Biochim. Biophys. Acta* 2000; **1475**: 133.
11. Parapini S, Basilico N, Pasini E, Egan TJ, Olliaro P, Taramelli D, Monti D. *Exp. Parasitol.* 2000; **96**: 249.
12. Adams PA, Berman PAM, Egan TJ, Marsh PJ, Silver J. *J. Inorg. Biochem.* 1996; **63**: 69.
13. Nguyen-Cong V, Rode BM. *J. Chem. Inf. Comput. Sci.* 1996; **36**: 114.
14. Bolboaca M, Kiefer W, Popp J. *J. Raman Spectrosc.* 2002; **33**: 207.
15. Puviarasan N, Arjunan V, Mohan S. *Turk. J. Chem.* 2004; **28**: 53.
16. Krishnakumar V, Ramasami R. *Spectrochim. Acta, Part A* 2005; **61**: 673.
17. Cînta Pînzaru S, Leopold N, Pavel I, Kiefer W. *Spectrochim. Acta, Part A* 2004; **60**: 2021.
18. Frosch T, Küstner B, Schlücker S, Szeghalmi A, Schmitt M, Kiefer W, Popp J. *J. Raman Spectrosc.* 2004; **35**: 819.
19. Bayden Wood R, Langford SJ, Cooke BM, Lim J, Glenister FK, Duriska M, Unthank JK, McNaughton D. *J. Am. Chem. Soc.* 2004; **126**: 9233.
20. Bayden Wood R, Langford S, Cooke B, Glenister F, Lim J, McNaughton D. *FEBS Lett.* 2003; **554**: 247.
21. Kneipp K, Kneipp H, Bhaskaran Kartha V, Manoharan R, Deinum G, Itzkan I, Ramachandra Dasari R, Feld MS. *Phys. Rev., E* 1998; **57**: 6281.
22. Cotton TM, Kim JH, Chumanov GD. *J. Raman Spectrosc.* 1991; **22**: 729.
23. Kneipp K, Kneipp H, Itzkan I, Dasari RR, Feld MS. *Curr. Sci.* 1999; **77**: 915.
24. Sutherland WS, Winefordner JD. *J. Colloid Interface Sci.* 1984; **99**: 270.
25. Moskovits M. *Rev. Mod. Phys.* 1985; **57**: 783.
26. Creighton JA. *Spectroscopy of Surface*, Clark RJH, Hester RE (eds). Wiley: New York, 1988; 37.
27. Champion A, Kambhampati P. *Chem. Soc. Rev.* 1988; **27**: 241.
28. Socrates G. *Infrared and Raman Characetristic Group Frequencies. Tables and Charts* (3rd edn). Wiley: 2001; 173.
29. Moskovits M, DiLella DP. *J. Chem. Phys.* 1980; **73**: 6068.
30. Moskovits M, Suh JS. *J. Phys. Chem.* 1988; **92**: 6327.
31. Crisanti MA, Spiro TG, English DR, Hendrickson DN, Suslik KS. *Inorg. Chem.* 1984; **23**: 3897.
32. Smulevich G, Spiro TG. *J. Phys. Chem.* 1985; **89**: 5168.
33. Choi S, Spiro TG, Langry KC, Smith KM, Budd DL, La Mar GN. *J. Am. Chem. Soc.* 1982; **104**: 4345.
34. Otto A. *J. Raman Spectrosc.* 2002; **33**: 593.

3. Bulboaca2002 (truncated)

Vibrational characterisation of coordination and biologically active compounds by means of IR absorption, Raman and surface-enhanced Raman spectroscopy in combination with theoretical simulations

Dissertation

zur Erlangung des
naturwissenschaftlichen Doktorgrades
der Bayerischen Julius-Maximilians Universität Würzburg

vorgelegt von

Monica-Maria Bolboaca

aus

Cluj-Napoca, Rumänien

Würzburg 2002

obtain a deeper understanding of the vibrational spectra of complicated molecules. Recently it was shown that density functional theory (DFT) methods are a powerful computational alternative to the conventional quantum chemical methods, since they are much less computationally demanding and take account of the effects of electron correlation [14, 15].

Due to its non-destructive character Raman spectroscopy became during time an invaluable tool in the study of the structure of biologically active molecules. However, the application of conventional Raman spectroscopy is limited by the weak intensity of the Raman scattered light and the appearance of fluorescence. One way to overcome these disadvantages is the use of surface-enhanced Raman spectroscopy (SERS) [16-18]. Although the theoretical understanding of the mechanism of surface enhancement is not definite and still evolving, the experimental data accumulated in the last years has demonstrated SERS to be a sufficiently sensitive spectroscopic method for surface science, analytical applications and biophysics [19].

In the present work, a background of the spectroscopic methods and theoretical calculations is summarized in Chapters 2 and 3. Structural characterisations of various coordination compounds by means of infrared absorption and Raman spectroscopy in combination with density functional theory calculations are presented in Chapter 4. In section 4.1 experimental (infrared and FT-Raman spectroscopy) and theoretical (density functional theory calculations) investigations are performed on the starting materials Ph_2P-N(H)$SiMe_3$ and $Ph_3P{=}NSiMe_3$ and their corresponding $[(MeSi)_2NZnPh_2P$-$NSiMe_3]_2$ and $Li(o\text{-}C_6H_4PPh_2NSiMe_3)]_2{\bullet}Et_2O$ complexes in order to find out how the P–N bond is affected by the coordination to the metal center. In the next subsections (4.2 and 4.3) two series of hexacoordinated silicon(IV) and germanium(IV) complexes with three symmetrical bidentate oxalato(2-) and unsymmetrical bidentate hydroximato(2-) ligands, respectively, are investigated using FT-Raman and infrared absorption spectroscopy in conjunction with density functional theory calculations in order to elucidate their vibrational spectra. In section 4.2 kinetic investigations of the hydrolysis of two trisoxalato complexes, one with silicon and another one with germanium, are performed at room temperature and at different pH values, while in the

Lebenslauf

Persönliche Daten

Name	Monica-Maria Bolboaca
Geboren am	31.08.1974
in	Cluj-Napoca
Familienstand	ledig

Ausbildung und Beruf

Schulbildung	1981 - 1985	Grundschule, Cluj-Napoca
	1985 – 1989	M. Eminescu Gymnasium, Cluj-Napoca
	1989 – 1993	Theoretisches Gymnasium Nr. 1 , Cluj-Napoca
Abitur	Juni 1993	
Studium	1993-1997	Physikstudium an der Babes-Bolyai Universität Cluj-Napoca
	Juni 1997	Lizenzprüfung
	1997 – 1998	Masterstudium Biophysik und Medizinische Physik an der Babes-Bolyai Universität Cluj-Napoca
	Juni 1998	Abschlussprüfung
	1998 – 1999	Masterstudium Atomphysik and der Babes-Bolyai Universität Cluj-Napoca
	Juni 1999	Abschlussprüfung

Promotion	Okt. 1999	Beginn der Promotion am Lehrstuhl für Physikalische Chemie II der Universität Würzburg bei Prof. Dr. Wolfgang Kiefer
Anstellungen	Okt. 1999 – Dez. 2001	Wissenschaftliche Mitarbeiterin im Sonderforschungsbereich 347 der Deutschen Forschungsgemeinschaft
	seit Jan. 2002	Wissenschaftliche Mitarbeiterin

Acta Cryst. (1988). C**44**, 1605–1608

Redetermination of the Crystal and Molecular Structure of the Antimalarial Chloroquine Bis(dihydrogenphosphate) Dihydrate

BY JEAN M. KARLE*

Department of Pharmacology, Division of Experimental Therapeutics, Walter Reed Army Institute of Research, Washington, DC 20307-5100, *USA*

AND ISABELLA L. KARLE

Laboratory for the Structure of Matter, Naval Research Laboratory, Washington, DC 20375-5000, *USA*

(*Received* 12 *December* 1987; *accepted* 18 *April* 1988)

Abstract. N^4-(7-Chloro-4-quinolinyl)-N',N'-diethyl-1,4-pentanediamine bis(dihydrogenphosphate) dihydrate, $C_{18}H_{28}ClN_3^{2+}.2H_2PO_4^-.2H_2O$, $M_r = 551{\cdot}8$, monoclinic, $P2_1/c$, $a = 9{\cdot}830\ (2)$, $b = 16{\cdot}879\ (3)$, $c = 15{\cdot}783\ (4)$ Å, $\beta = 105{\cdot}51\ (2)°$, $V = 2523{\cdot}2$ Å^3, $Z = 4$, $D_x = 1{\cdot}452$ g cm^{-3}, Mo $K\alpha$, $\lambda = 0{\cdot}71073$ Å, $\mu = 2{\cdot}78$ cm^{-1}, $F(000) = 1168$, room temperature, final $R = 5{\cdot}5\%$ for 2431 reflections with $|F_o| > 3\sigma$. The chloroquine molecule is a dication with a hydrogen atom from each of the phosphate moieties residing on the quinoline and the terminal chain nitrogen atoms. Neighboring phosphate chains are bridged by chloroquine molecules *via* hydrogen bonding. Each hydrogen atom on each nitrogen atom, on each phosphate oxygen atom, and in each water molecule participates in hydrogen bonding. The helical manner in which the side chains of the chloroquine molecules wrap around phosphate chains and the stacking interval of the quinoline rings between the phosphate groups may be indicative of the interaction of chloroquine molecules with cellular constituents important to antimalarial action.

Introduction. Chloroquine (Fig. 1), first developed for human use during World War II, was the drug of choice for the treatment of *Plasmodium falciparum* (Webster, 1985). However, in the 1960's resistant strains of *P. falciparum* appeared in Asia and South America which have now spread across all of the

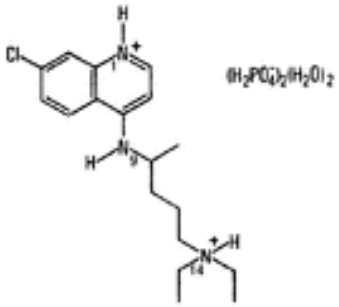

Fig. 1. Chemical structure of title compound.

* To whom correspondence should be addressed.

0108-2701/88/091605-04$03.00